Six circumpolar currents

– on the forcing of the Antarctic Circumpolar Current by wind and mixing

Dirk Olbers, Karsten Lettmann and Ralph Timmermann

Alfred Wegener Institute for Polar and Marine Research, 27515 Bremerhaven, Germany

revised 8th June 2006

Abstract

The transport of the Antarctic Circumpolar Current (ACC) is influenced by a variety of processes and parameters. A proper implementation of basin geometry, ocean topography and baroclinicity is known to be a fundamental requisite for a realistic simulation of the circulation and transport. Other, more subtle parameters are those of eddy-induced transports and diapycnal mixing of thermohaline tracers or buoyancy, either treated by eddy resolution or by a proper parameterization. Quite a number of realistic numerical simulations of the circulation in the Southern Ocean have recently been published. Many concepts on relations of the ACC transport to model parameters and forcing function are in the discussion, however, without much generality and little success.

We present a series of numerical simulations of circumpolar flow with a simplified numerical model, ranging from flat-bottom wind-driven flow to baroclinic flow with realistic topography and wind and buoyancy forcing. Analysis of the balances of momentum, vorticity and baroclinic potential energy enables us to develop a new transport theory, which combines the most important mechanisms driving the circulation of the ACC and determining its zonal transport. The theory is based on the importance of the bottom vertical velocity in generating vorticity and shaping the baroclinic potential energy of the ACC. It explains the breaking of the f/h-constraint by baroclinicity and brings together in one equation the wind and buoyancy forcing of the current. The theory emphasizes the role of Ekman pumping and eddy diffusion of buoyancy to determine the transport. It also demonstrates that eddy viscosity effects are irrelevant in the barotropic vorticity balance and that friction arises via eddy diffusion of density. In this regime, the classical Stommel model of vorticity balance is revived where the bottom friction coefficient is replaced by K/λ^2 (with the GM coefficient K and the baroclinic Rossby radius λ) and a modified wind curl forcing appears.

1. Introduction

What are the mechanisms and forcing functions that set the zonal transport of the Antarctic Circumpolar Current (ACC)? Early, mostly unsatisfying attempts to approach this central issue of research on the ACC used barotropic dynamics in a flat-bottom ocean (e.g. Hidaka and Tsuchiya 1953, Gill 1968). In general – i.e. with reasonably sized eddy viscosities – they predicted far too high transports. But inclusion of a realistic or idealized bottom relief did not provide circulations with more realistic transports since these were generally far too weak

(e.g. Johnson and Hill 1975, Klinck 1991, Krupitsky and Cane 1994, Wang and Huang 1995, Krupitsky *et al.* 1996). Analytical models with baroclinicity are rare. Some could relate the transport to the windstress at least in the correct order of magnitude (e.g. Johnson and Bryden 1989, Marshall *et al.* 1993, Olbers and Völker 1996, Krupitsky and Cane 1997, Völker 1999; for recent reviews see Rintoul *et al.* 2001 and Olbers *et al.* 2004). Other recent transport relations are based on scaling (e.g. Karsten *et al.* 2002, Olbers 2005) or derived from analysis of numerical models with eddy resolution (e.g. Olbers and Ivchenko 2001).

The transition from the flat-bottom regime with high transport to smaller, realistic values in a baroclinic ocean with topography is an outstanding result of numerical circulation modeling. The importance of the geostrophic contours, baroclinicity and topography were demonstrated in a series of early numerical experiments with the GFDL model of the world ocean circulation. As central experiments in this model area we deem the studies of Bryan and Cox (1972) and Cox (1975) of which we will describe some details below. In addition, there is an enormous wealth of global simulations with coarse grid ocean models (e.g. Cai and Baines 1996, Gent *et al.* 2001). An extensive study with simplified geometry is reported by Gnanadesikan and Hallberg (2000). All these attempts with numerical models could generally not verify dependencies of the ACC transport on forcing functions, as proposed by scaling or analytical concepts. What clearly emerged from these studies, however, is that the ACC transport depends not only on the amplitude of the zonal windstress, but also on properties of its meridional structure such as the wind curl or the Ekman pumping. It also depends on the surface fluxes of heat and freshwater, on the implementation of mixing, and especially on the shape of the marine topography.

In the present study we use a numerical ocean circulation model to address the question of forcing circumpolar transport in a new approach. While the forcing functions and the geometry and topography are realistic as in most other numerical simulations with coarse ocean models, the physics of the present ocean model (the BARBI model, see Olbers and Eden 2003) are extremely simplified to the basic dynamical processes. They are implemented in the vertically integrated equations for momentum, vorticity and potential energy: the integrated barotropic and baroclinic pressure forces in the momentum balance, the resulting pressure torques in the vorticity balance of the vertically averaged velocity, and the processes which shape the vertically integrated baroclinic potential energy, namely mechanisms that induce lifting of stratified water in an ocean with topography, and processes that tend to flatten isopycnals. The potential energy becomes a prognostic variable in BARBI because it generates JEBAR (Joint Effect of Baroclinicity And bottom Relief, Sarkysian and Ivanov 1971). JEBAR is a prominent source of vorticity in addition to the windstress curl and flow across the geostrophic contours in a vertically averaged view of the flow. The simplicity of the BARBI physics allows us to reveal some fundamental compensation mechanisms in the balances of vorticity and potential energy and to route the forcing through the model equations. Our aim is to derive a unified 'transport equation' which combines the most important dynamical processes and forcing functions in one balance equation.

The paper is organized as follows. Section 2 gives a short introduction into the physics of the BARBI model (further details can be found in the appendices). We have performed six simulations with BARBI in a circumpolar configuration with different combinations of forcing functions (wind and surface density flux), topography (flat ocean or realistic bottom relief) and treatment of baroclinicity. The simulations differ substantially, they partly even have reversed forcing functions. The resulting circumpolar currents are described and analyzed in section 3.1, with emphasis on the local balances of depth-integrated momentum and vorticity,

and the baroclinic potential energy. Finally, in section 4 we utilize our findings on the local balances of vorticity and potential energy to derive the 'transport equation' which reveals the forcing mechanisms (wind curl, Ekman pumping and small-scale mixing) in relation to the dynamical ingredients (vorticity dynamics and eddy advection of density). The last section is a concluding discussion of our findings. In the course of this study we refer to dynamical concepts (such as bottom formstress, bottom torque, JEBAR, and eddy diffusion) which operate in the BARBI physics. Short explanations are outlined in the Appendices A and B.

2. The BARBI model

The model used in this study is a two-mode version of the BARBI model (BARotropic-Baroclinic-Interaction ocean model, Olbers and Eden 2003). The physics of this model can be summarized by the set of equations

$$\frac{\partial \mathbf{U}}{\partial t} + f\mathbf{k}\times\mathbf{U} = -h\boldsymbol{\nabla}P - \boldsymbol{\nabla}E + \boldsymbol{\tau} + \mathbf{F} \tag{1}$$

$$\frac{\partial E}{\partial t} + h\mathbf{U}\cdot\boldsymbol{\nabla}\frac{E}{h^2} - \frac{1}{2}N^2\boldsymbol{\nabla}\cdot\left[\tilde{\mathbf{u}} + \frac{1}{3}\mathbf{U}h^2\right] = \mathcal{Q} - \mathcal{D} + K\nabla^2 E \tag{2}$$

$$\frac{\partial \tilde{\mathbf{u}}}{\partial t} + f\mathbf{k}\times\tilde{\mathbf{u}} = \frac{1}{3}h^2\left[\boldsymbol{\nabla}E - \boldsymbol{\tau}\right] + \tilde{\mathbf{F}} \tag{3}$$

These are the balances of the vertically integrated velocity $\mathbf{U}$, the baroclinic potential energy E, and a baroclinic velocity moment $\tilde{\mathbf{u}}$, defined by

$$\mathbf{U} = \int_{-h}^{0}\mathbf{u}\,dz \qquad E = g\int_{-h}^{0} z\rho\,dz \qquad \tilde{\mathbf{u}} = \int_{-h}^{0} z^2(\mathbf{u}-\mathbf{U}/h)dz \tag{4}$$

Furthermore, $P = g\zeta + g\int_{-h}^{0}\rho dz$ is the bottom pressure associated with the surface displacement ζ and the mass stratification contained in ρ which is a perturbation density about a mean background stratification described by the Brunt-Väisälä frequency N. This is taken constant in this study. Finally, h is the ocean depth, $\boldsymbol{\tau}$ is the windstress, and $\mathcal{Q}$ is a buoyancy source described below. All densities, pressures and stresses are scaled by a constant reference density. We will refer to $\mathbf{U}$ as transport velocity but frequently also as transport. The rigid lid approximation implies $\boldsymbol{\nabla}\cdot\mathbf{U} = 0$ so that we may represent $\mathbf{U}$ by the streamfunction of the volume transport, $\mathbf{U} = \mathbf{k}\times\boldsymbol{\nabla}\psi$. The lateral friction term[1] in (1) is $\mathbf{F} = A\boldsymbol{\nabla}\cdot h\boldsymbol{\nabla}(\mathbf{U}/h)$ with a constant eddy viscosity A. Note that there is no bottom friction. In the balance of the second vertical moment $\tilde{\mathbf{u}}$ of the baroclinic horizontal velocity we have a friction term $\tilde{\mathbf{F}}$ which derives from lateral momentum diffusion.

Equation (2) is the balance of baroclinic potential energy referred to the surface. It is derived from the thermohaline balance (see Appendix B, equation (26)) and neglects the baroclinic self-advection (advection of density by the baroclinic velocity $\mathbf{u} - \mathbf{U}/h$ and associated vertical velocity). Note that the advection of the background density field is retained. The balance (2) contains a dissipation term $\mathcal{D}$ which destroys potential energy, and an eddy

[1]We loosely use the terminus 'friction' for the diffusion of momentum (and vorticity) though friction is only acting at boundaries by this term.

diffusion term with constant diffusivity K. The motivations behind these terms are given in Appendix B where both are derived from a Gent-McWilliams parameterization of eddy fluxes. In the simulations of this study we use the simple form $\mathcal{D} = \mu E$ to relax towards a state with flat isopycnals (with a constant inverse time scale μ). The Q-forcing of potential energy in the BARBI model is given by the vertical integral of the vertical turbulent buoyancy transport,

$$\mathcal{Q} = g \int_{-h}^{0} \overline{w'\rho'} dz \tag{5}$$

which includes both subgrid mixing and convection. We shall refer to the Q-forcing as buoyancy forcing. We use the familiar boundary conditions for advective-diffusive ocean models: kinematic condition and no-slip for $\mathbf{U}$ and $\tilde{\mathbf{u}}$ and no-flux for E at solid boundaries.

We like to point out that most terms in the above balances result exactly by vertical integration of the primitive equations. However, the BARBI system has a closure to utilize $\mathbf{U}, E$ and $\tilde{\mathbf{u}}$ as complete set of state variables[2]. It has, on the other hand, no restriction on the height or slope of topography. Formally, the system describes two modes of planetary-topographic waves (including advection) which are driven by a windstress $\boldsymbol{\tau}$ and a source $\mathcal{Q}$ of potential energy from surface buoyancy flux and small scale mixing processes in the water column. A linear wave analysis shows that BARBI has the familiar set of mixed barotropic-baroclinic Rossby waves of topographic-planetary dynamics (see e.g. Rhines 1977).

Note that the windstress appears twice as forcing in the BARBI equations. First, we have the direct forcing of vertically integrated momentum (or transport) in (1). Second, there is wind forcing in the baroclinic momentum balance (3) as well. Routing this effect through the equations we learn that transport may be forced indirectly via the E-pressure gradient associated with wind acting via Ekman pumping on the mean stratification. Unraveling the importance of the different forcing function and the establishment of the ACC transport is the main issue of the present study.

3. Six experiments with BARBI

The experiments with BARBI extend a series of early numerical experiments with the GFDL model of the world ocean circulation. Bryan and Cox (1972) presented the circulation for a homogeneous fluid (constant density, thus having zero JEBAR) in an ocean with continents but constant depth. Cox (1975) extended the studies to the cases of variable topography and constant density, hence still zero JEBAR, and also to a topographic ocean with baroclinicity, hence nonzero JEBAR. Due to limited computer resources, the last experiment was largely a diagnostic simulation, i.e. the thermohaline fields do not deviate much from the initial state taken from hydrographic observations. But full prognostic experiments have since then been repeated many times (e.g. Han 1984a, 1984b, Olbers and Wübber 1991, Cai and Baines 1996) with similar results. Simulations with BARBI of these three cases are discussed in Olbers and Eden (2003).

[2]The closure mainly concerns the baroclinic pressure term in (3). For the present two-mode system we use a slightly different closure than outlined in Olbers and Eden (2003). The baroclinic Rossby radius of the BARBI equations is $\lambda = Nh/|f|/\sqrt{6}$. Because a flat-bottom baroclinic Rossby wave with constant BVF has a Rossby radius $\lambda = N_0 h/(|f|\pi)$ we take the N in the potential energy balance as an effective Brunt-Väisälä frequency (BVF) related to the real BVF N_0 by $N_0 = \pi N/\sqrt{6}$. This is the BARBI closure.

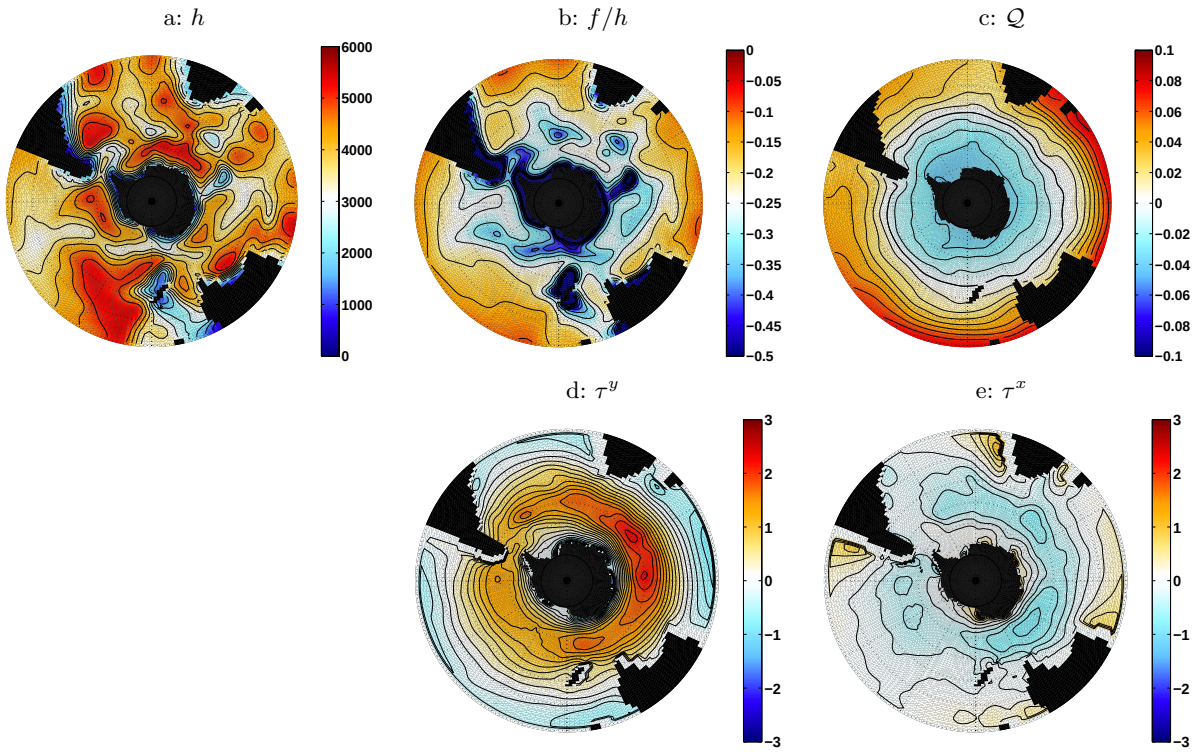

FIGURE 1. Model topography and forcing. a) depth h [m], b) geostrophic contours f/h [10^{-7} m^{-1}s^{-1}], c) the buoyancy forcing [10^{-4} m^{3}s^{-3}] in experiments QMX and WQMX, d) and e) the components of windstress [10^{-4} m^{2}s^{-2}].

3.1. Model set-up

The numerical experiments in this study model the circulation around Antarctica (south of 20°S), as established in a spin-up from a motionless state ($\mathbf{U} = \tilde{\mathbf{u}} = E = 0$) to a steady state. The horizontal resolution is $2^o \times 1^o$, the horizontal viscosity is $A = 4 \times 10^4$ m^{2}s^{-1}, the eddy diffusivity is $K = 4 \times 10^3$ m^{2}s^{-1}, and the dissipation coefficient of potential energy is $\mu = 1.5 \times 10^{-10}$ s^{-1}. The baroclinic cases have $N = 1.8 \times 10^{-3}$ s^{-1} which yields a baroclinic Rossby radius $\lambda = 21$ km. The model is forced with interpolated annual mean windstress data from the NCEP reanalysis, and a buoyancy forcing $\mathcal{Q}$ appearing in (2) and defined by (5). The topography was interpolated from the ETOPO20 dataset onto the model grid and smoothed with a two-dimensional symmetric filter. The Drake Passage of the model is open between 62.5°S and 55.5°S. Figure 1 shows the ocean depth h, the f/h-contours, the components of windstress, and the buoyancy flux $\mathcal{Q}$ for the experiments. The curl of the windstress can be found in Figure 12 and Figure 13.

Because the turbulent buoyancy flux $g\overline{w'\rho'}$ in the ocean interior is largely unknown we construct a Q-forcing from a fairly simple parameterization. We implement a down-gradient parameterization $\overline{w'\rho'} = -K_v d\bar{\varrho}/dz$ into (5), where $\varrho(z)$ is the profile of the mean total density. Integration yields

$$\mathcal{Q} = -gK_v \left[\varrho(z=0) - \varrho(z=-h)\right] \tag{6}$$

Experiment		Transport
wind-forced		
FL	flat bottom	1093
BT	barotropic (ρ=const; $N = 0$)	33
NL	nonlinear	102
NO	linear (no advection)	116
buoyancy-forced		
QMX	$\mathcal{Q}$ from flux param.	20
wind and buoyancy forced		
WQMX	$\mathcal{Q}$ from flux param.	120

TABLE 1. There are two suites of experiments: the cases FL, BT, NL and NO are purely wind-forced, and the cases QMX, and WQMX which incorporate buoyancy forcing.

The mean density is taken from the World Ocean Atlas (Levitus *et al.* 1994) and the diffusivity is chosen as $K_v = 3\times10^{-4}\,\mathrm{m^2 s^{-1}}$. To avoid unwanted small-scale features in near-coast regions the bottom density is replaced by a constant. The area mean is subtracted to define $\mathcal{Q}$ (see Figure 1) which is negative in the circumpolar belt and rises to positive values to the north. Following the effect of $\mathcal{Q}$ on $\boldsymbol{\nabla} E$ the mixing in the ocean implemented in QMX and WQMX propels an eastward flow.

3.2. Gross features of the ACC simulations

We present and discuss six wind- and buoyancy-driven simulations of circumpolar flow. Their outfit is briefly summarized in Table 1. The streamfunctions are depicted in Figure 2, the fields of potential energy, and bottom pressure in Figures 3 and 4 (shown only for some experiments, see figure captions), respectively. The flat-bottom, homogeneous case (FL) has an ACC transport of about 1100 Sverdrups (there are more than 600 Sv in Bryan and Cox 1972). The homogeneous ocean with topography (BT) has very low ACC transport (22 Sv in Cox 1975, 33 Sv in BARBI). The third experiment (NL), now considering baroclinic conditions in a topographic ocean, has a realistic transport for the ACC (187 Sv in Cox 1975, 102 Sv in BARBI, compared to about 140 Sv through Drake Passage from observations, see e.g. Rintoul *et al.* 2001 and Olbers *et al.* 2004). Some discussion of these simulations of circumpolar currents is given in Olbers *et al.* (2004). The fourth wind-driven experiment (NO) is BARBI-specific and has no counterpart in previous work. NO uses a linearized version of the BARBI

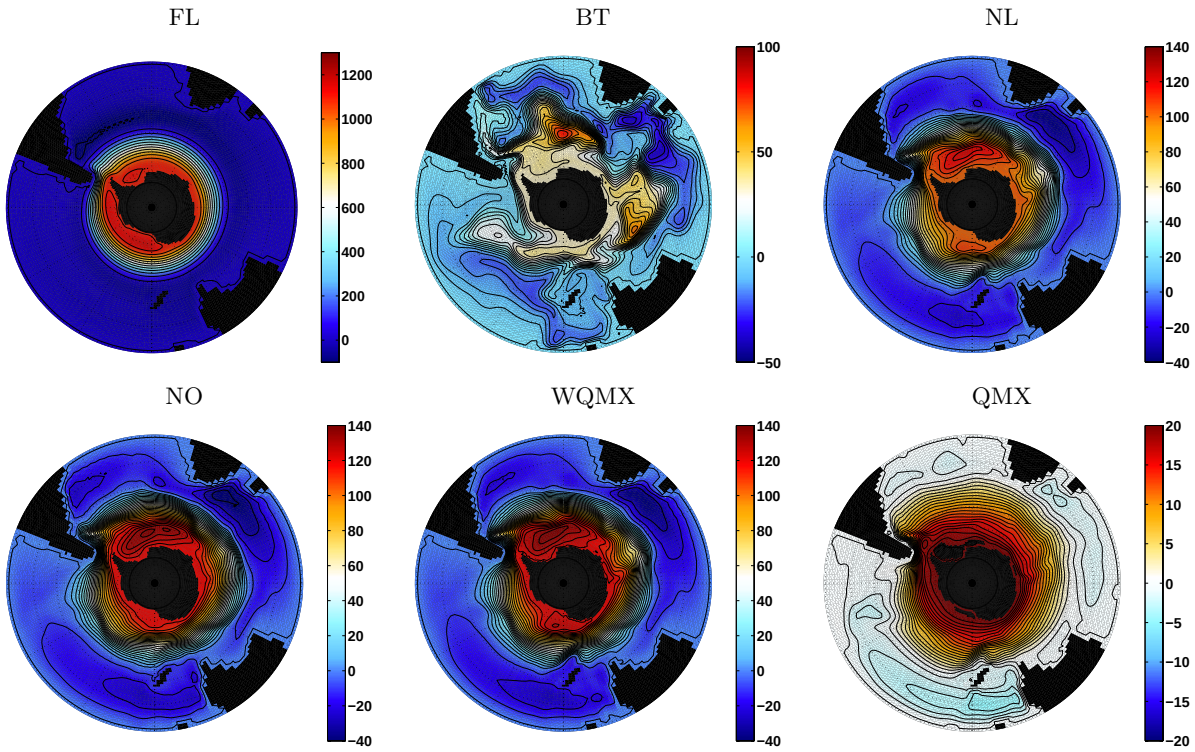

FIGURE 2. Streamfunctions obtained with the *BARBI* model forced by wind-stress and buoyancy forcing. a) FL: homogeneous flat-bottom ocean. b) BT: using realistic topography. c) NL: simulation including baroclinicity. d) NO: same as case c) but without advection. e) WQMX: simulation with wind and buoyancy forcing MX. f) QMX: simulation with buoyancy forcing MX only. Units: Sv, CI = 100 Sv for FL and 10 Sv for the other experiments.

equations (the advection term in (2) is omitted), resulting in a circumpolar current with great similarity to the complete nonlinear case NL. The NO-transport is 116 Sv.

There are two simulations which have a buoyancy forcing: QMX is only forced by the source $\mathcal{Q}$ in the potential energy balance (2) and WQMX has wind and buoyancy forcing applied. The transports are 20 Sv in QMX, and 120 Sv in WQMX. The buoyancy forcing thus adds transport almost linearly to the underlying wind-driven part. The WQMX case has a close resemblance to NL. A short description of the circulation patterns in the six ACCs follows. More details (the balances of momentum, vorticity, and potential energy) of these six wind-driven and buoyancy-forced ACC-like currents are described in the following sections. We like to mention that experiments with alternative buoyancy forcing have been performed in which $\mathcal{Q}$ decreases towards the north. Then the buoyancy forced part of the transport is found to be westward.

The flat-bottom case FL has an almost zonal ACC. There is slight squeezing of streamlines in Drake Passage and a marked northward shift behind that obstacle in the path of the current. The contours of potential energy (which is passive in this simulation) and pressure are similar. Since bottom formstress cannot operate, friction is the only momentum sink.

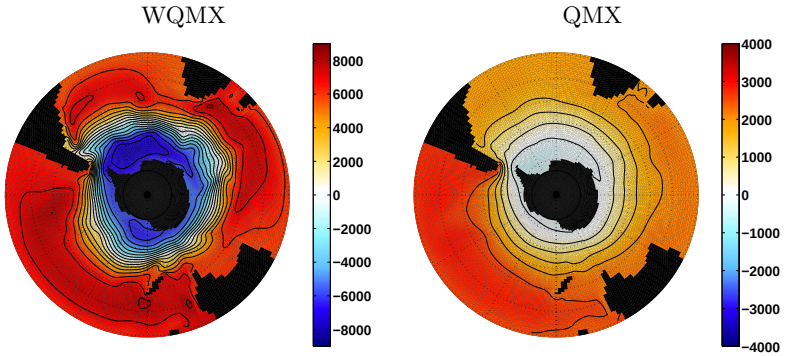

FIGURE 3. Potential energy for the cases WQMX and QMX. Units: m^3s^{-2}, CI = 1000 m^3s^{-2} for WQMX and 500 m^3s^{-2} for QMX.

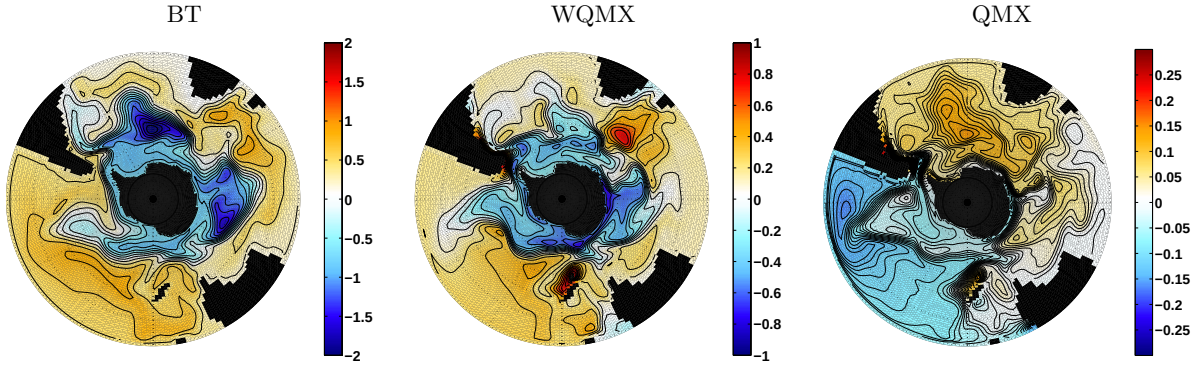

FIGURE 4. Bottom pressure for the cases BT, WQMX and QMX. Units: m^2s^{-2}, CI = 0.2 m^2s^{-2} for BT, 0.1 m^2s^{-2} for WQMX, and 0.01 m^2s^{-2} for QMX.

With the diffusive parameterization of lateral eddy-induced transports of momentum by a diffusivity A, the zonal transport is roughly proportional to $Y^3\tau_0/A$ where Y is the width of the current. We are facing 'Hidaka's dilemma' (Hidaka and Tsuchiya 1953, see Wolff *et al.* 1991): either we implement a reasonably sized diffusivity (as in the present set-up) and then get an unrealistically large transport or we must use an unrealistically large eddy viscosity to get a reasonable size of the ACC transport.

The topographic case with homogeneous density, BT, has a transport that is far too low to represent ACC conditions. The system now establishes a bottom formstress and a bottom pressure torque (but not JEBAR) from the surface pressure being out-of-phase with the submarine barriers of the flow (see Figure 4b, a detailed analysis follows in section 3.3). The current is mostly along those geostrophic contours (compare Figures 2 and 1b) which are north of the Drake Passage belt. Embedded in the circumpolar flow are huge closed circulation cells above the Midatlantic Ridge and around the Kerguelen plateau.

The cases NL, NO and WQMX, which consider topography and baroclinicity get reasonably sized circumpolar flow with little apparent influence of the underlying topography. Note that the potential energy follows quite closely the streamlines while the bottom pressure has

a tendency to follow the f/h contours and has some resemblance to the barotropic state BT (though there are marked differences between all these cases). An explanation is given in section 3.4.2. Surprisingly, there are no obvious structural differences between the nonlinear case NL and the linear case NO. In particular, the latter case shows a similar northward jump of the flow behind Drake Passage which therefore is neither inertial (there is no inertia in the model at all) nor advective. It must be attributed to topographic and stratification effects. All three cases show a distinct Weddell Sea gyre and a weak Ross Sea gyre. The buoyancy-driven case QMX has a similar circumpolar circulation pattern as the cases with wind driving but much smaller transport. The meridional gradient of potential energy is much weaker in these ACCs than in those with wind driving applied.

3.3. The overall balance of momentum

Most investigations of circumpolar dynamics emphasize the zonally integrated balance of zonal momentum because the most obvious driving agent – the windstress vector – shows a dominantly zonal direction. We follow this route initiated by Munk and Palmén (1951), before we consider local balances. Zonal integration (denoted by angle brackets) of the zonal component of the momentum balance (1) yields[3]

$$\langle \tau^x \rangle - \langle h P_x \rangle + \langle F^x \rangle - \Delta E \Big|_{continents} = 0 \tag{7}$$

With topography present and restricted to the latitude belt of Drake Passage this is the well-known 'form-drag' balance (see e.g. Olbers *et al.* 2004 and references therein) between input of eastward momentum by the zonal windstress (the first term) and loss by bottom formstress (the second term). Friction (the third term) only plays a significant role over a flat-bottom ocean, and the pressure force acting on the continents (the fourth term) is only working if the zonal path is interrupted by continents. Note that in case of homogeneous density the ΔE-term is absent. There is also a ΔP-contribution from $\langle h P_x \rangle$ because in the model topography the ocean depth does not go to zero at the coasts. The balance for the basic six experiments is displayed in Figure 5.

In the belt of latitudes which pass through Drake Passage we find the 'form-drag balance' between windstress and bottom formstress (except for clear reasons in FL). Outside this belt the balance is mainly between windstress and the pressure difference on the continents (ΔE and $h\Delta P$). This, in fact, is the principle balance of momentum in the basin-wide gyre circulations embedded between continents. Note that the eastward flow in QMX is formstress-driven, not only in the Drake Passage belt but also in the ACC and the gyres to the north and the subpolar domain.

The bottom formstress arises from a systematic phase shift of the pressure P with respect to the underlying topography h. To obtain a net westward acceleration of the eastward current, highs of P must appear to the west and lows to the east of topographic barriers in the path of the flow. In fact, the flow organizes such that this sink of eastward momentum can become effective. Figure 6 displays the bottom pressure at a central latitude through Drake Passage together with the corresponding ocean depth, and in a similar way for a latitude north of Drake Passage. The shaping of the formstress is apparent: in the Drake Passage belt we notice a westward shift of roughly 10° of P with respect to h and no such (or a less correlated) pattern

[3]We simplify equations by use of local Cartesian coordinates. All data evaluations of the BARBI model are performed in spherical coordinates. Lower indices denote derivatives, upper indices denote vector components.

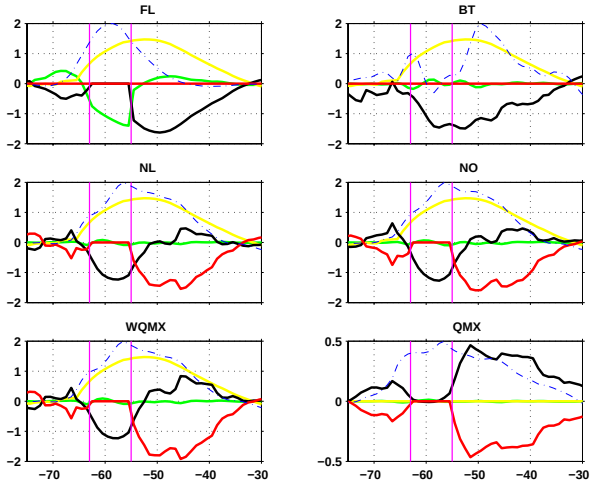

FIGURE 5. Zonally integrated momentum balance as function of latitude for all cases. Drake Passage is indicated by purple lines. Windstress: yellow, bottom formstress: black, friction: green, pressure difference on continents: red. The dotted blue curve is the profile of the mean zonal velocity. Units: 10^{-4} m^{2}s^{-2}.

at latitudes to the north. Only case QMX is different in most parts because here the formstress accelerates eastward, and we find a low in P more or less westward to the topographic highs.

3.4. Local balances

We continue with the analysis of the local balances of momentum, vorticity and potential energy. The linear case NO is only mentioned in passing because differences to NL are small for the diagnostics established here. In the balances of momentum and vorticity we do not see great differences between NL and WQMX (corresponding figures are almost indistinguishable). Consequently, we will show only results for WQMX.

3.4.1. BALANCE OF MOMENTUM The flow in all cases is, of course, predominantly in geostrophic balance. Thus, deviations from this are of interest. In a zonal channel with a flat bottom, where the current is almost zonal and zonal pressure gradients are negligible, we have geostrophy in the meridional balance and only frictional terms in the zonal balance,

$$fU \approx -h\frac{\partial P}{\partial y} \qquad \tau^x + A\frac{\partial^2 U}{\partial y^2} \approx 0 \tag{8}$$

These equations serve as the simplest ACC model. They show that the transport is determined by ageostrophic terms which set up the zonal balance while the pressure must adjust according to geostrophy. In a realistic geometry, with the continental barriers of South America and the Antarctic Peninsula, the ACC heads north after passing Drake Passage, and there, strong zonal pressure gradients can develop. It is meaningful to consider the momentum balance in streamline coordinates (s along ψ-contours and n normal; note that $U_\perp \equiv 0$). Then, for the case FL, we find in the normal component again geostrophy dominating to at least an order of magnitude but in the parallel component the pressure gradient plays a major role. Thus in

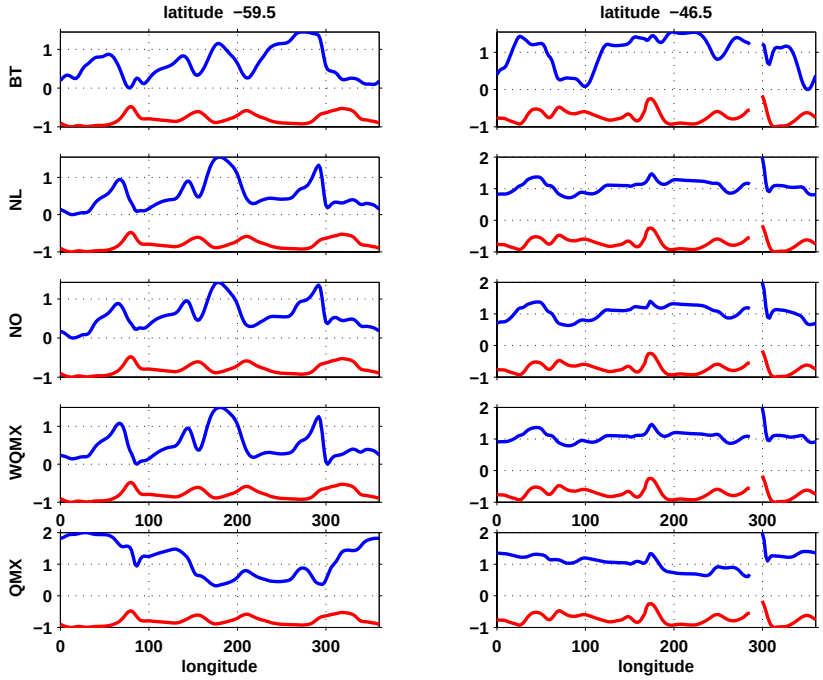

FIGURE 6. Bottom pressure – depth correlation as a function of longitude for two sets of latitudes and all cases except FL. The left column is for a latitude in Drake Passage, the right column is for a more northern latitude. Bottom pressure: upper curves [blue], ocean depth: lower curves [red]. Scaled (depth is shown as $-h/max(h)$, pressure is shown by $P/max(|P|)+1$).

$$-h\frac{\partial P}{\partial s}+\tau_{\|}+F_{\|}\;=\;0 \tag{9}$$

the friction term $F_{\|}$ is small north of Drake Passage and the along-streamline balance there is much like the one of a subtropical gyre. Clearly, in the latitude band of Drake Passage, friction builds up and plays a major role in the balance. Nevertheless, unlike the flat bottom case (8), the pressure now has an active role in shaping the current.

The circulation of the barotropic case BT is mostly along the geostrophic contours f/h. These contours are expelled from Drake Passage due to a high sill, and flow around Antarctica is only of marginal size. The response of the ocean to the winds occurs mostly in form of closed gyres around topographic features. The balance of the normal component is now highly geostrophic (at least two orders of magnitude dominant, see Figure 7). In the parallel component the wind input is positive on the northern part of the large localized gyres and negative on the southern part and correspondingly balanced by the along-contour pressure gradient (see Figure 8). Friction is an order of magnitude smaller and occurs very localized.

The role and relative size of the terms in the complete nonlinear cases (NL and WQMX) are similar to BT. However, their patterns are completely different because the current now runs around Antarctica in a quite realistic 'quasi-zonal' stream. The flow is geostrophic as

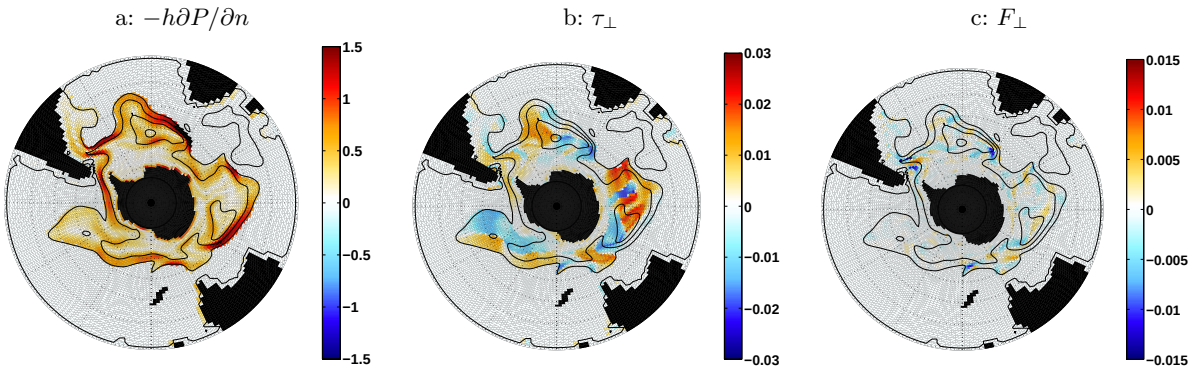

FIGURE 7. Local momentum balance normal to streamlines for case BT. a) normal gradient of bottom pressure (the corresponding Coriolis force is indistinguishable from this figure). b) normal component of windstress. c) normal component of friction term. Units: 10^{-2} m^{2}s^{-2}. The contours show the streamfunction, CI = 25 Sv.

before (see Figure 9) but now with respect to the sum of the two pressure gradients, $-h\partial P/\partial n$ and $-\partial E/\partial n$. The balance of the parallel component of momentum is between pressure and windstress. There is surprisingly little effect from the friction (see Figure 10).

The structure of the individual pressure terms is shown in Figure 11. The normal gradients are of similar size. However, the bottom pressure gradient term is very localized, occurring in worm-like features oriented at the streamlines, whereas the E gradient term is a broad scale structure. It has an imbedded filamented pattern which just compensates the bottom pressure worms, so that the total pressure force becomes smoother. This behavior can be expected because P is diagnosed from the Poisson equation (23) with smooth E and ψ terms.

3.4.2. BALANCE OF VORTICITY The pressure forces enter the balance of vorticity as a torque-like term. There are two forms of vorticity. The vorticity balance of the depth integrated momentum **U** is

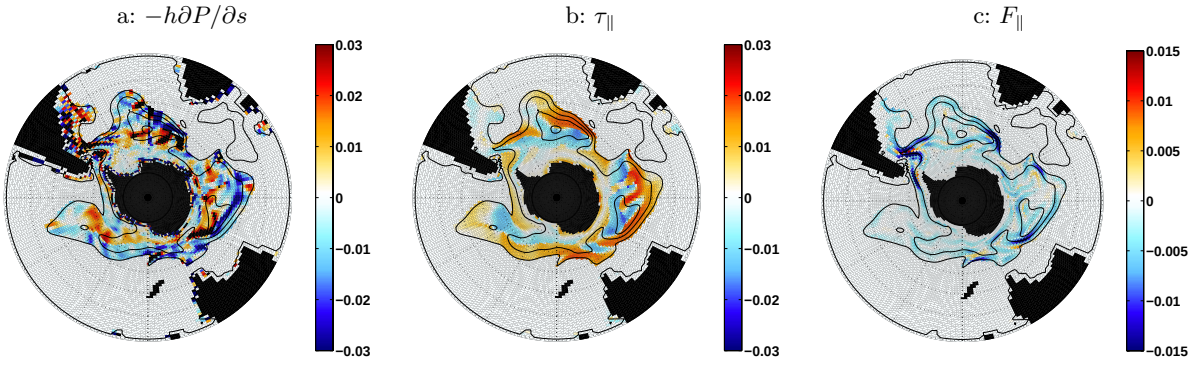

FIGURE 8. Local momentum balance parallel to streamlines for case BT, corresponding to Figure 7 (there is no Coriolis term). Units: 10^{-2} m^{2}s^{-2}. The contours show the streamfunction, CI = 25 Sv.

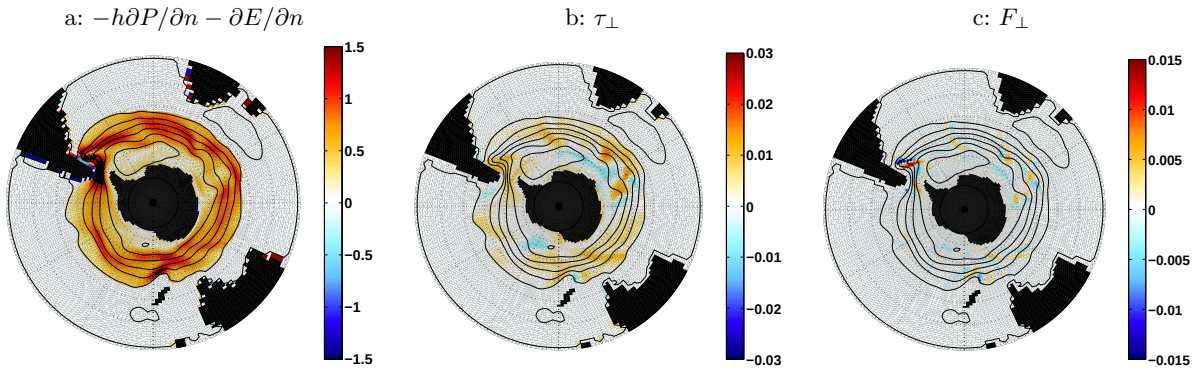

FIGURE 9. Local momentum balance normal to streamlines for case WQMX. Units: 10^{-2} m^{2}s^{-2}. The contours show the streamfunction, CI = 25 Sv.

$$\frac{\partial}{\partial t}\boldsymbol{\nabla}^2\psi + \beta\frac{\partial\psi}{\partial x} \;=\; \mathcal{J}(P,h) + \text{curl}\;\boldsymbol{\tau} + \text{curl}\;\mathbf{F} \tag{10}$$

Here, $\mathcal{J}(P,h)$ appears as source of vorticity. It has become custom to refer to it as *bottom torque* (Holland 1973). The other form of vorticity equation is built from (1) by elimination of the pressure P,

$$\frac{\partial}{\partial t}\boldsymbol{\nabla}\cdot\frac{1}{h}\boldsymbol{\nabla}\psi + \mathcal{J}\left(\psi,\frac{f}{h}\right) \;=\; \mathcal{J}(E,\frac{1}{h}) + \text{curl}\;\frac{\boldsymbol{\tau}}{h} + A\blacktriangledown^4\psi \tag{11}$$

It describes the balance of vorticity of the depth-averaged velocity $\mathbf{U}/h$. It is forced by another torque-like term, $\mathcal{J}(E,1/h)$, the JEBAR term (Joint Effect of Baroclinicity And bottom Relief) of Sarkysian and Ivanov (1971). The nabla-4 operator $\blacktriangledown^4$ is similar to the familiar ∇^4,

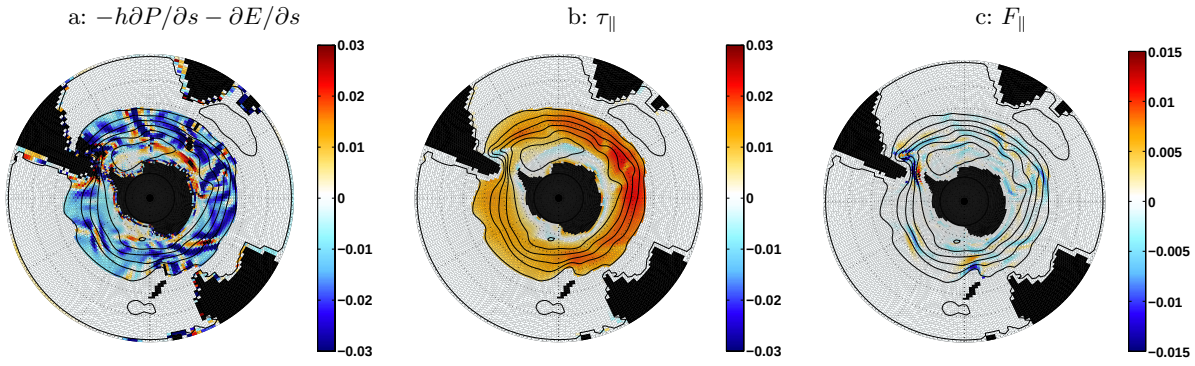

FIGURE 10. Local momentum balance parallel to streamlines for case WQMX. Units: 10^{-2} m^{2}s^{-2}. The contours show the streamfunction, CI = 25 Sv.

$$A\blacktriangledown^4\psi \;=\; \text{curl}\,\frac{\mathbf{F}}{h} \;=\; A\boldsymbol{\nabla}\cdot\left(\frac{1}{h}\boldsymbol{\nabla}\cdot h\boldsymbol{\nabla}\frac{1}{h}\right)\boldsymbol{\nabla}\psi \tag{12}$$

but modified by the depth h. The vorticity balance of the depth-averaged velocity can be taken as one of the prognostic equations of the BARBI model (supplemented the integral constraint (25), see Appendix B), replacing the momentum balance (1) and the mass balance.

Both vorticity equations have drawn much attention in dynamical considerations of the ocean circulation. Many studies have emphasized the different characteristics in these balances (latitude circles in (10) and the geostrophic contours f/h-contours in (11)) and their connection to the forcing by the different wind curls and the pressure torques. There is a long-lasting discussion (see e.g. the summaries in Olbers 1998 and Olbers *et al.* 2004) to what degree the ACC is in a Sverdrup balance, i.e. whether the vorticity balances (10) and (11) are dominated by the appropriate curl of the windstress and the advection of planetary or planetary-topographic vorticity (referring to the β-term in (10) or the Jacobian $\mathcal{J}(\psi, f/h)$ in (11)). It will be demonstrated that none of the present solutions are in a Sverdrup or modified Sverdrup regime. Understanding the role of these terms in the circumpolar dynamics is a major issue of the present study.

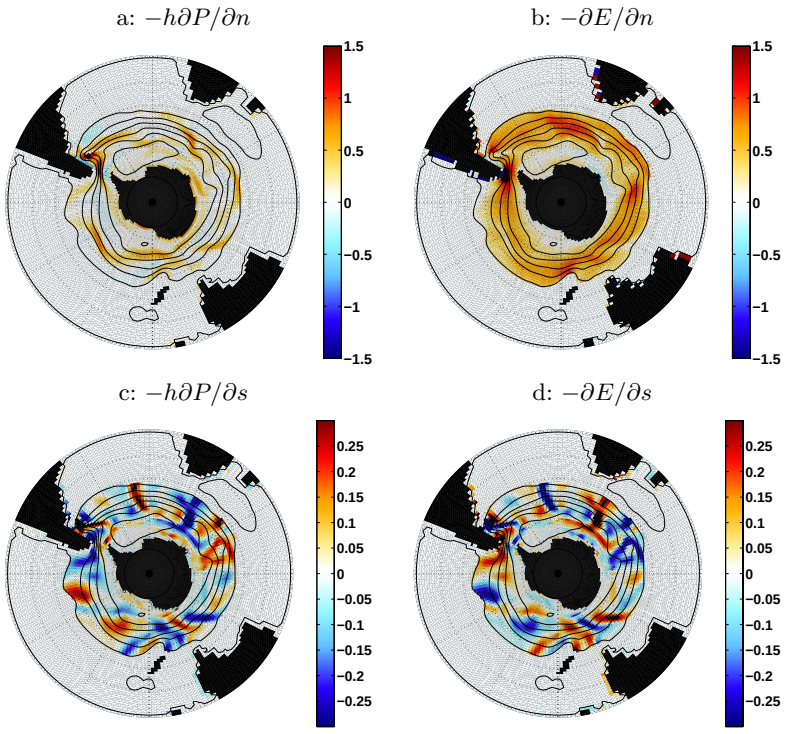

FIGURE 11. The pressure gradient terms normal and parallel to streamlines for case WQMX. a) and b): normal gradients. c) and d): parallel gradients. Units: 10^{-2} m^{2}s^{-2}. The contours show the streamfunction, CI = 25 Sv.

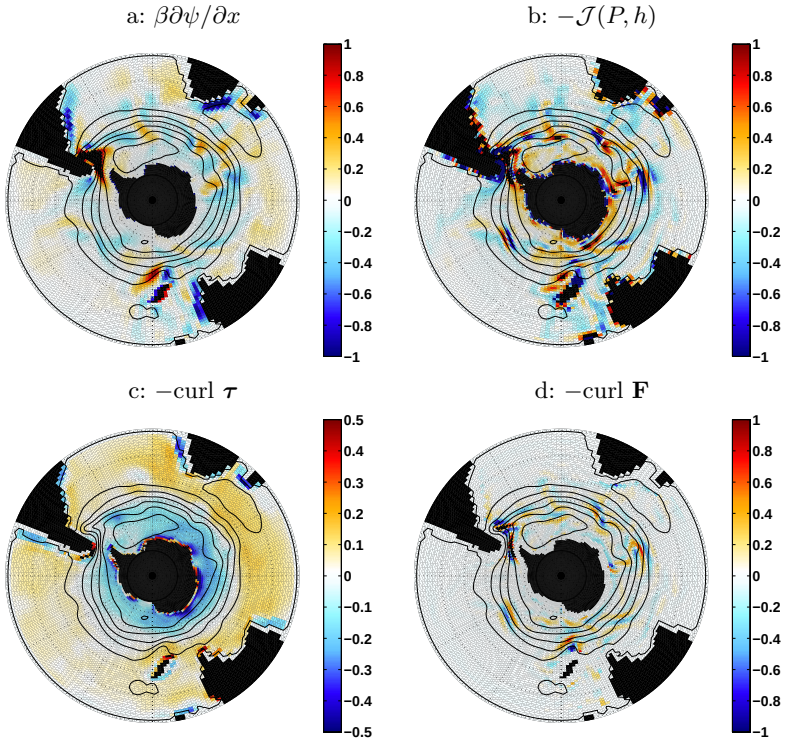

FIGURE 12. Vorticity balance of depth-integrated current for case WQMX. a) β-term. b) bottom torque. c) curl of windstress. d) friction term. Units: 10^{-9} ms^{-2}. The contours show the streamfunction, CI = 25 Sv.

For a flat bottom the two vorticity balances collapse. Because the current in FL squeezes before Drake Passage and turns northward after passing it (this occurs in all solutions) the β-term cranks up before and after the passage (strong advection of planetary vorticity) and we find it balanced by friction. This balance is also found in the remaining area, with contribution from the wind curl, though all terms there have a considerably smaller size (not shown).

With varying topography the bottom torque comes into play in (10) and dominates the depth-integrated balance in the cases BT, NL, NO and WQMX. In BT where the current tends to follow f/h-contours we naturally find a strong β-term which is largely compensated by the bottom torque, in agreement with the study of Hughes and de Cuevas (2001). Friction is generally small and contributes only locally where the current converges. The wind curl is small. In the depth-averaged balance (11) of BT the β-term and the bottom torque combine to the advection term of planetary-topographic vorticity (because the flow is basically geostrophic) and now, we find a balance between this term and friction.

In the baroclinic solutions NL, NO, Q1 and WQMX the f/h-constraint is overcome by the introduction of baroclinicity and the flow becomes almost zonal. The importance of the β-term in (10) reduces with an exception after Drake Passage and some other areas where the current must deviate from zonal due to islands or other massive changes in the topography. The depth-integrated balance is now between bottom torque and friction with contribution from the windstress curl (see Figure 12). It is then not surprising that the dominant terms in

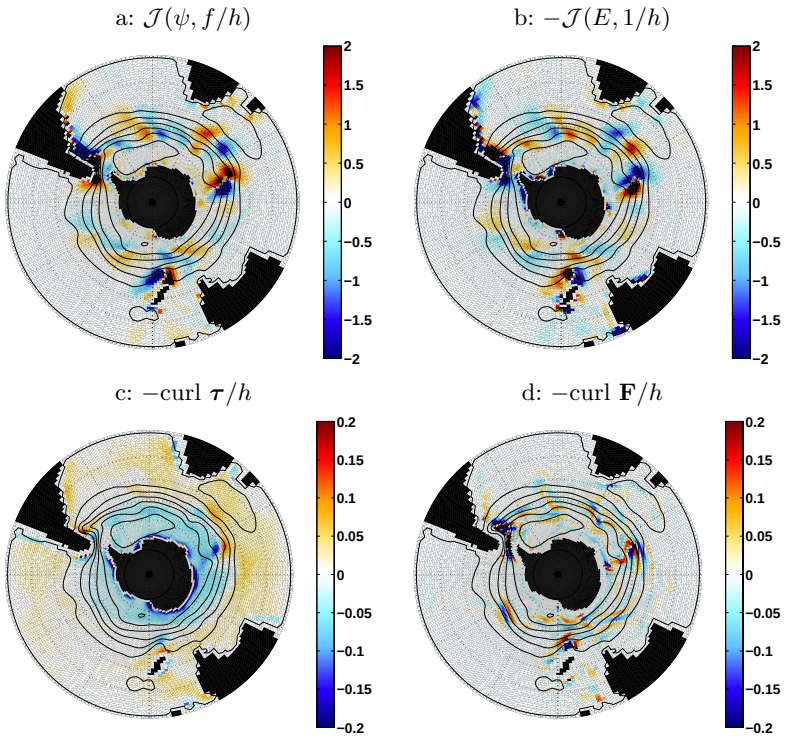

FIGURE 13. Vorticity balance of depth-averaged current for case WQMX. a) topographic-planetary β-term. b) JEBAR. c) curl of windstress. d) friction term. Units: 10^{-12} s^{-2}. The contours show the streamfunction, CI = 25 Sv.

the depth-averaged balance (11) are – by at least an order of magnitude – the topographic-planetary Jacobian and the JEBAR term. They largely oppose and cancel each other, as obvious from Figure 13. Wind and friction are an order of magnitude smaller. Again, this is a reflection of predominance of the geostrophic terms in the balance of momentum. As shown above, the P term is more localized so that we have in all baroclinic solutions roughly $f\boldsymbol{\nabla}\psi \approx \boldsymbol{\nabla}E$ over most of the domain. This was already pointed out by Borowski *et al.* (2002) and Borowski (2003).

The occurrence of large compensating terms in a dynamical balance indicates that the problem is imprudently formulated. For the baroclinic solutions it appears sensible to combine the planetary-topographic Jacobian and the JEBAR into one expression to achieve a cancelation of dominating geostrophic terms, as previously proposed by Mellor *et al.* (1982) and Greatbatch *et al.* (1991). An obvious choice is $\psi - E/f$ which combines the streamfunction of the total transport with a streamfunction-type variable E/f. We find

$$\mathcal{J}(\psi, \frac{f}{h}) - \mathcal{J}(E, \frac{1}{h}) \;=\; \mathcal{J}(\psi - \frac{E}{f}, \frac{f}{h}) - \frac{\beta}{f}\frac{\partial(E/h)}{\partial x} \tag{13}$$

Both terms on the rhs of these relations are much smaller than each individual term on the lhs (not shown). Alternatively one may use the torque exerted by pressure-like variable $f\psi - E$.

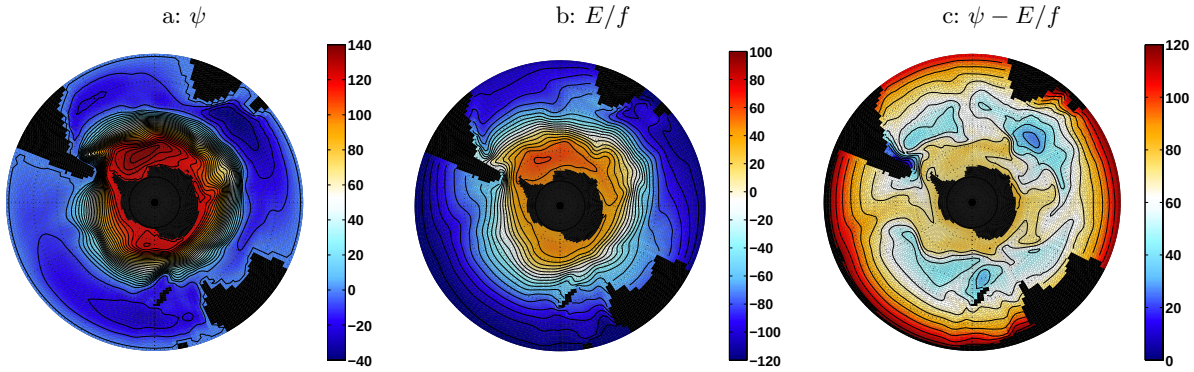

FIGURE 14. Streamfunction ψ (a) and quasi-streamfunctions E/f (b) and $\psi - E/f$ (c) for case WQMX. Units: Sv, CI = 10 Sv.

The new torques should behave smoother in numerical simulations. In summary, we state that JEBAR is mathematically a correct concept but physically not sound.

There is a physical interpretation of the variables appearing in the Jacobian on the rhs of (13). In Appendix A we note that E is the pressure of the geostrophic transport relative to the bottom, $\mathbf{U}_g - h\mathbf{u}_g(-h)$, and E/f may be viewed as its streamfunction. Thus, $\psi - E/f$ is associated with $\mathbf{U} - \mathbf{U}_g + h\mathbf{u}_g(-h) = \mathbf{U}_{ag} + h\mathbf{u}_g(-h)$. Consequently, in a geostrophic approximation, we may interpret $\psi - E/f$ as a (quasi-)streamfunction of the bottom-related geostrophic transport $h\mathbf{u}_g(-h)$ and $(f/h)(\psi - E/f)$ as the pressure field associated with the geostrophic bottom velocity $\mathbf{u}_g(-h)$. Remembering that P is the pressure which is approximately in geostrophic balance with $\mathbf{u}_g(-h)$ we find then that $P \sim (f/h)(\psi - E/f)$ should approximately hold. This explains the resemblance of P with the geostrophic contours f/h found in the simulations (see section 3.2). The (quasi-) streamfunctions $-E/f$ and $\psi - E/f$ are depicted in Figure 14. According to the pattern found, the deep flow occurs in three large cells under the path of the ACC.

3.4.3. BALANCE OF POTENTIAL ENERGY The baroclinic simulations use the potential energy balance (2) to predict the baroclinic state in the BARBI model. The balance (3) of the baroclinic velocity moment may in fact be taken diagnostically and implemented into (2) to yield

$$\frac{\partial E}{\partial t} + h\mathbf{U}\cdot\boldsymbol{\nabla}\frac{E}{h^2} + \frac{N^2}{6}\left[\mathcal{J}(E,\frac{h^2}{f}) - \mathcal{J}(\psi,h^2)\right] = \\ = \mathcal{Q} - \frac{N^2}{6}\mathrm{curl}\,\frac{h^2\boldsymbol{\tau}}{f} - \mathcal{D} + K\nabla^2 E \tag{14}$$

This equation immediately reveals that the potential energy is not only generated by the buoyancy forcing $\mathcal{Q}$ and internal redistributions of mass. The latter occurs by advecting the background stratification by the baroclinic geostrophic velocity and the barotropic velocity induced by the bottom variations. There is also another external source, namely the lifting and lowering of the background stratification by the Ekman pumping. These processes act against the dissipation and diffusion terms which operate towards a state of uniform E. Comparing

the terms on the rhs of (14) we can judge (without any model integration) whether buoyancy forcing in the presence of wind would be effective in generating transport: $(\mathcal{Q}/f)/\lambda^2$ must exceed curl $\boldsymbol{\tau}$. Here $\lambda = |Nh/f|/\sqrt{6}$ is the baroclinic Rossby radius.

The potential energy balance suffers from the dominance of the geostrophic terms in a similar way as the vorticity balance. While the geostrophic terms entered there as almost compensating torques, they come into the balance of potential energy as integrals of vertical velocities which largely cancel each other. We may rephrase the statement about the dominance of the geostrophic terms as one about a partial compensation of the bottom-induced vertical barotropic velocity and the geostrophic vertical baroclinic velocity. In (2) the contributions from the variables $\tilde{\mathbf{u}}$ and $h^2\mathbf{U}/3$, entering the divergence in (2), are large in the simulations and largely cancel each other (see Figure 15). We show in Appendix B that their sum, $\mathbf{v} = \tilde{\mathbf{u}} + h^2\mathbf{U}/3$, can be viewed as the bottom velocity. The divergence is the vertical velocity at the bottom which is small compared to its baroclinic and barotropic constituents. A remedy for this problem is to abandon gravity waves and use (14) to predict the potential energy. As in the reformulation of the vorticity equation given above, the pumping terms in this form should be rewritten in terms of either $\psi - E/f$ or $f\psi - E$.

It was mentioned before that the linear solution NO does not differ much from the nonlinear counterpart NL. Omitting the advection term in the potential energy balance only changes the big players in the divergence term slightly without much affecting the structure of the fields. The orientation of the E-contours in NL and NO in an almost zonal form is clearly not the effect of advection but rather due to the wind forcing in form of the Ekman pumping term in (14).

The balance (14) of the potential energy allows to put the equations of the BARBI model into a more familiar environment, the dynamics of a two-layer quasigeostrophic model. Indeed, (11) corresponds to the QG balance of the depth-integrated vorticity if the nonlinear advection terms are abandoned there as well. Furthermore, if the QG balance of the baroclinic vorticity (upper minus lower layer streamfunctions) is considered for scales exceeding the baroclinic Rossby radius we find a close similarity to the above balance (14) of potential energy, with E/f as baroclinic geostrophic streamfunction (see e.g. Borowski 2003). There is term by term correspondence except for the dissipation and friction terms: the baroclinic QG balance has a viscosity term in addition to the layer thickness diffusion which is contained in the BARBI equation. There are differences because BARBI is valid for arbitrary topography height and slope while QG needs infinitesimal slopes. An important difference between BARBI and QG concerns the handling of the geostrophic terms. Whereas the vorticity equation in the QG approach only contains ageostrophic terms both above outlined vorticity equations (and the balance of potential energy as well) do not use a geostrophic approximation and thus still have the basic geostrophic balance terms implemented. As mentioned, this leads to some of the features discussed in this section.

4. The baroclinic Stommel transport equation

In the previous sections we have shown that the above balances are dominated by the Jacobian terms in the experiments with baroclinicity, namely the ACC-like cases NL, NO, and WQMX. Clearly, to override the constraint imposed by the f/h characteristics such a state of almost zonal circulation is heavily depending on variations of the topography and the presence of baroclinicity. We may use this knowledge to solve the balance of potential energy for E

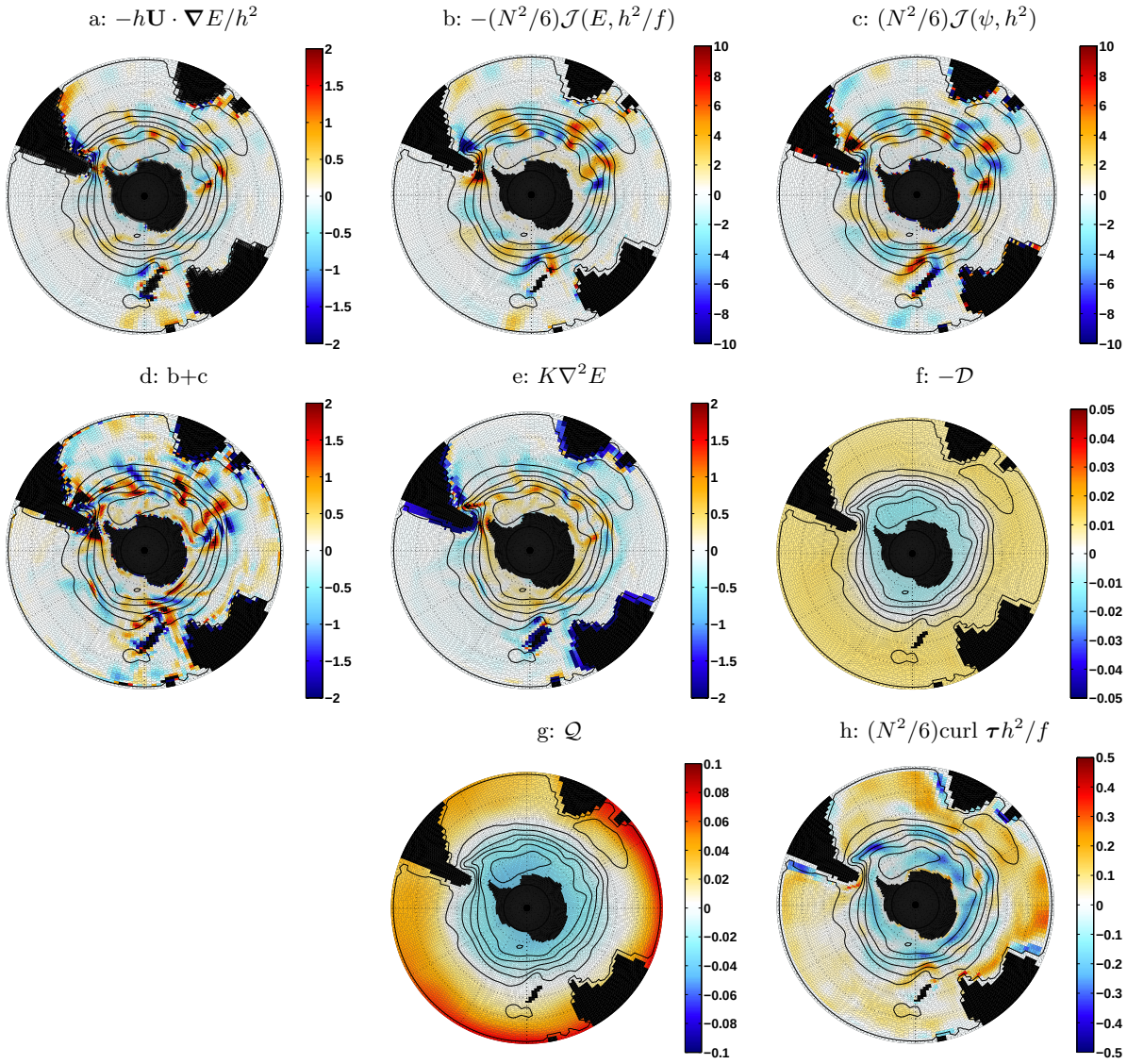

FIGURE 15. Terms of the potential energy balance (14) for case WQMX. a) advection. b) barotropic divergence term c) baroclinic divergence term. d) net divergence term. e) eddy diffusion term. f) dissipation term. g) buoyancy forcing. h) Ekman pumping term. Units: 10^{-4} m^{3}s^{-3}. The contours show the streamfunction, CI = 25 Sv.

and eliminate the JEBAR term together with its compensating partner from the planetary-topographic Jacobian in the vorticity balance. Circulation states in which topography is not important are easily envisioned, e.g. the flat-bottom case FL as the extreme limit. We may also consider the limit of weak stratification, $N^2 \to 0$, in which the E-balance must be governed by advection and diffusion. These regimes, however, have little resemblance with the ACC which has stratification and strong bottom variations.

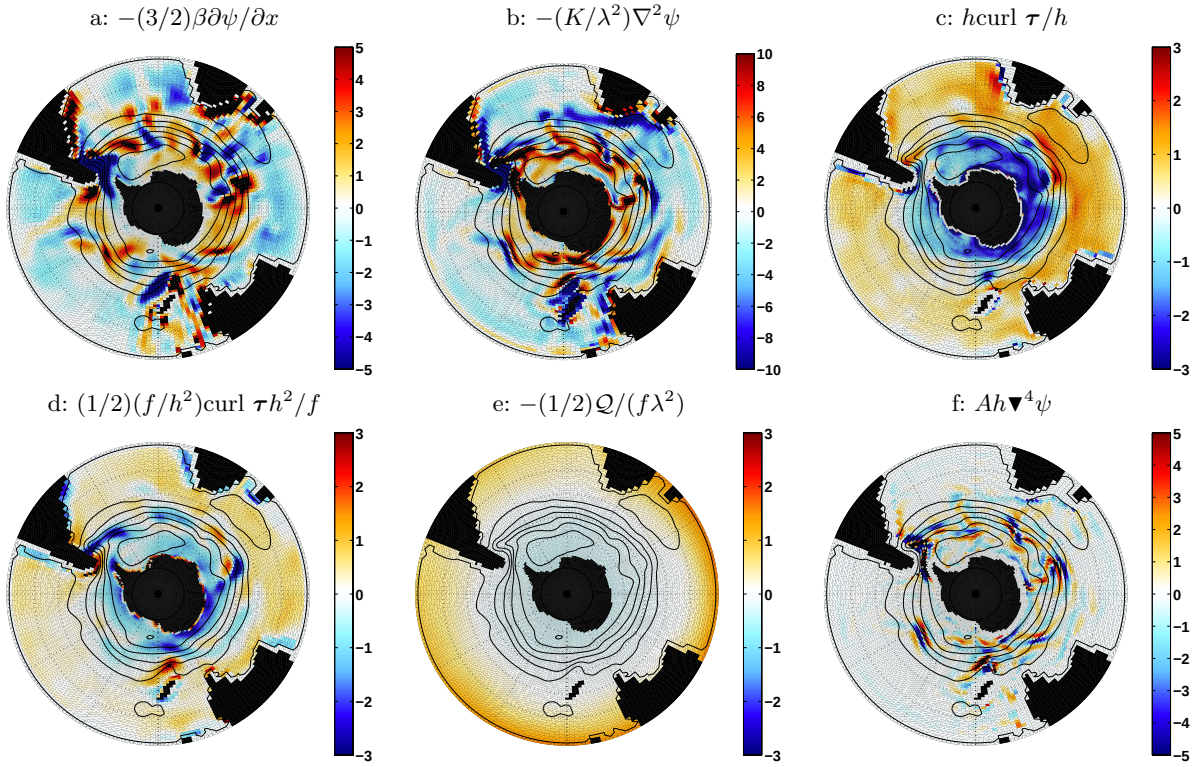

FIGURE 16. Forcing terms in the transport equation (17). a) β-term. b) eddy diffusion term. c) curl of windstress. d) Ekman pumping term. e) buoyancy forcing. f) viscous diffusion term. Units: 10^{-10} ms^{-2}. The contours show the streamfunction, CI = 25 Sv.

Using the above described findings of canceling terms in (11) and (14) we intend to derive an overarching transport theorem. We assume steady conditions and weak advection. After some small rearrangements the balance of E is cast into the form

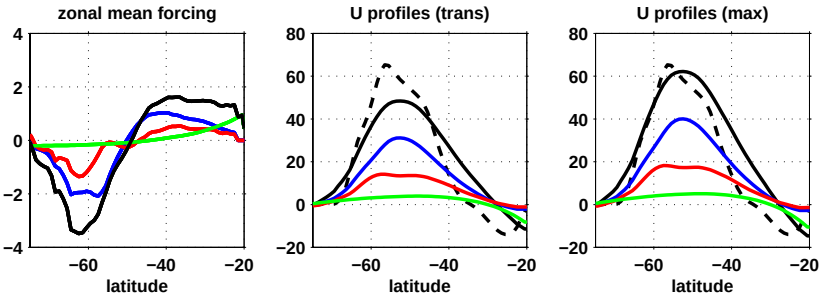

FIGURE 17. Left: Zonal mean forcing terms [10^{-10} ms^{-2}] in the transport equation (17) [black: total, blue: direct wind, red: Ekman pumping, green: buoyancy forcing]. Middle and left: Profiles of zonal mean velocity $\bar{U}$ [m^{2}s^{-1}] for different forcing terms. [same colors, black dashed: profile from WQMX].

$$(15) \qquad \frac{1}{2hf}\left[\beta\frac{\partial E}{\partial x}+\kappa\nabla^2 E\right]+\mathcal{J}(E,\frac{1}{h}) \;=\; f\mathcal{J}(\psi,\frac{1}{h})-\frac{\mathcal{Q}-\mathcal{D}}{2fh\lambda^2}+\frac{f}{2h^3}\,\mathrm{curl}\,\frac{h^2\boldsymbol{\tau}}{f}$$

with $\kappa = K/\lambda^2 = 6Kf^2/(N^2h^2)$. This general form of the potential energy balance is clearly not accessible to exact analytical solutions. In the ACC case the main terms in the balance are the Jacobians. We identify the small parameters $\beta L/f$ and $\kappa/f = K/(\lambda^2 f)$. To lowest order in these parameters the Jacobians in (15) cancel each other and we have $E \approx f\psi + const.$ Inserting this result into the remaining small terms we thus get, summed to the first order,

$$(16) \qquad \mathcal{J}(E,\frac{1}{h}) \;=\; f\mathcal{J}(\psi,\frac{1}{h})-\frac{1}{2h}\left[\beta\frac{\partial\psi}{\partial x}+\kappa\nabla^2\psi\right]-\frac{1}{2h}\left[\frac{\mathcal{Q}-\mathcal{D}}{f\lambda^2}-\frac{f}{h^2}\,\mathrm{curl}\,\frac{h^2\boldsymbol{\tau}}{f}\right]$$

The combined vorticity – potential energy balance thus becomes

$$(17) \qquad \frac{3}{2}\beta\frac{\partial\psi}{\partial x}-Ah\blacktriangledown^4\psi+\frac{K}{\lambda^2}\nabla^2\psi \;=\; h\,\mathrm{curl}\,\frac{\boldsymbol{\tau}}{h}+\frac{1}{2}\frac{f}{h^2}\,\mathrm{curl}\,\frac{h^2\boldsymbol{\tau}}{f}-\frac{1}{2}\frac{\mathcal{Q}-\mathcal{D}}{f\lambda^2}$$

This is the most important result of this study. Several features are worth emphasizing. The evaluation of JEBAR switches off the f/h-characteristics in the vorticity balance and introduces f-contours as a controlling agent. Furthermore, we are faced with a new friction term and new forcing functions for the transport streamfunction. The lateral diffusion of potential energy leads to a term mimicking bottom friction, with a friction coefficient (inverse time scale) $f^2K/(N^2h^2)$ which actually is a reformulation of the eddy diffusivity into a vertical eddy viscosity (see e.g. Rhines and Young 1982, Olbers *et al.* 1985). For the parameters in the present simulations the corresponding term in (17) exceeds the viscous term by two orders of magnitude, $(K/A)(L/\lambda)^2 \sim 10^2$ where L is a typical size of the meridional scale. In addition to the wind curl, representing the direct effect of wind forcing, the Ekman pumping term and the buoyancy forcing appear. The pattern and magnitude of all terms in (17) are shown in Figure 16. The newly introduced vertical eddy viscosity term in the balance (17) is of baroclinic origin. It clearly dominates and is balanced by the β-term, the wind curl term associated with the direct wind driving in the momentum balance, and – with decreasing importance – by the Ekman pumping term, the buoyancy forcing and viscous diffusion (see also the zonal mean of these terms shown in Figure 17). The similarity of (17) to the classical Stommel model is obvious but here the friction derives from baroclinic eddy processes and part of the forcing comes from baroclinic processes as well.

It is tempting to simplify (17) even further. Discarding the viscous term and taking the zonal integral we arrive at

$$(18) \qquad \frac{K}{\lambda_0^2}\frac{\partial\langle U\rangle}{\partial y} \approx -\frac{\langle\mathcal{S}h^2/f^2\rangle}{h_0^2/f_0^2} \approx \;\langle\mathcal{S}\rangle$$

where $\mathcal{S}$ collects the forcing terms on the rhs of (17) (a constant Rossby radius $\lambda_0 = |Nh_0/f_0|/\sqrt{6}$ is introduced). Integration with $\bar{U} = 0$ at the southern boundary yields the current profile and the transport follows by further integration. The result for case WQMX is shown in Figure 17. There are two evaluations from (18): in the left panel we attempt

to reproduce the total transport of the zonal current (this is achieved with $\lambda_0 = 21$ km). In the right panel we aimed at the amplitude of the current (here we took a slightly larger Rossby radius, $\lambda_0 = 25$ km). It is obvious that the simple model is quite successful but gets increasingly worse at latitudes to the north of Drake Passage. There the ignored terms become important, in particular terms $\sim \Delta V$ arising from integrating the zonal part of the Laplacian of the 'bottom friction' term (V is the meridional transport velocity).

5. Summary and conclusions

We have analyzed a series of experiments with the ocean circulation model BARBI for the ACC, demonstrating and quantifying the important role of topography and stratification in determining the transport. Though extremely reduced in its physical contents, BARBI has the relevant ingredients to predict reasonable transport values from the applied forcing functions and simulate the transition from the flat-bottom regime with high transport to smaller, realistic values in a baroclinic ocean with topography. These ingredients are: realistic topography with blocking of the geostrophic contours; baroclinicity to generate baroclinic pressure gradients and corresponding torques in the vorticity dynamics; reaction of the stratified water columns to Ekman pumping and to flow over topography by inducing (barotropic and baroclinic) vertical velocities; and realistic forcing by windstress and buoyancy flux due to mixing in the ocean interior and a rough representation of interior mixing. We have implemented eddy fluxes of density from a GM approach (Gent and Williams 1990) and thus have a remnant of residual circulation physics even in the vertically integrated outfit of the BARBI model. The advantage gained by the reduced physics of BARBI is that we can go beyond merely analyzing results of the simulations. We use the simplicity of the few two-dimensional model equations to reveal the relation between forcing and transport.

Our experiments span a wide range of different dynamical regimes: a flat-bottom case, a barotropic case with topography, a linear and a nonlinear (with density advection) case with baroclinicity and wind forcing, and simulations which have a buoyancy source to generate gradients of baroclinic potential energy and hence transport. The analysis of the (local) balances of momentum and vorticity uncover several unexpected results. The wind driving is clearly dominant. In all experiments the friction terms (i.e. diffusion of momentum and vorticity) are fairly small and have very localized patterns although our diffusion parameters are fairly large, as required by a coarse resolution model. The current is thus in a geostrophic balance to a high degree, in particular with respect to the baroclinic pressure gradient arising from the potential energy variable. This property makes a prominent fingerprint in the vorticity balance where the advection of planetary-topographic vorticity f/h and the baroclinic JEBAR torque dominate by far the wind forcing and friction and therefore almost balance. We show that the relevant physical mechanism of (vertically averaged) vorticity generation is not found in the representation by vertically integrated quantities (the streamfunction of total transport in the planetary-topographic Jacobian and the potential energy in JEBAR) but rather in the vertical geostrophic velocity at the bottom. We suggest an alternative splitting of the planetary-topographic and JEBAR torques.

A similar situation is found in the balance of the vertically integrated potential energy (which generates JEBAR). The main sources are found in the pumping by vertical motions acting on the mean stratification, and here the pumping by barotropic and geostrophic baroclinic motions dominate by far and almost balance, followed in the score of importance by

Ekman pumping and the eddy diffusion. The latter largely oppose each other which is consistent with a partial cancelation of the Ekman and eddy-induced overturning in the residual circulation. Here, in close correspondence to the vorticity balance, the cancelation of the barotropic and baroclinic pumping is an indication that the pumping is rather due to the bottom velocity. Consequently we propose an alternative representation of the terms in the potential energy balance.

Finally, noting from the above analysis of balances that the barotropic and baroclinic prognostic variables of BARBI – namely the transport streamfunction and the baroclinic potential energy – are closely related (in fact in a linear form), we merge the depth-averaged vorticity balance and the balance of potential energy by a simple perturbation approach into an overarching equation which governs the streamfunction. It includes forcing from windstress and buoyancy flux, characteristics which follow latitude circles, and a new frictional term arising from the GM eddy density diffusion. This latter term has the flavor of bottom friction and clearly overwhelms the classical vorticity diffusion. The relevant friction coefficient derives from the eddy diffusivity K which is known to enter the residual form of the momentum balance as Kf^2/N^2. The theory may be seen as a reanimation of the classical Stommel model with the friction and part of the forcing arising from baroclinic processes.

We thus show how the f/h-constraint is broken by baroclinicity and f-contours are restored as governing characteristics, and that the lateral eddy viscosity is totally irrelevant for shaping the ACC transport. The transport of our topographic baroclinic simulations is thus roughly $\tau h^2 N^2/(Kf^2)$ times the width of the current for wind driving, and $\mathcal{Q}/(Kf)$ times square of the width for buoyancy driving. In our simulations the wind is far more effective – via direct forcing and via generating meridional gradients in the potential energy by Ekman pumping – than the buoyancy driving.

Acknowledgements We appreciate numerous discussions with Sergey Danilov, Carsten Eden, Richard Greatbatch, and Stephen Rintoul.

Appendix A. Pressure variables, formstress, JEBAR and bottom torque

The pressure terms in (1) arise from the vertical integration of the pressure gradient force $-\boldsymbol{\nabla} p$ in the horizontal balance of momentum,

$$\mathbf{F}_p = -\int_{-h}^{0} dz \boldsymbol{\nabla} p \; = \; -h\boldsymbol{\nabla} P - \boldsymbol{\nabla} E \tag{19}$$

Consequently, two pressure gradient forces enter the balance of vertically integrated momentum, as shown in (1). Associated with the two pressure gradient terms are geostrophic transports. The total is obviously given by

$$f\mathbf{k} \times \mathbf{U}_g \; = \; -h\boldsymbol{\nabla} P - \boldsymbol{\nabla} E \tag{20}$$

The bottom pressure P relates to the geostrophic velocity at the bottom,

$$f\mathbf{k} \times \mathbf{u}_g(-h) = -\boldsymbol{\nabla} P + g\rho(-h)\boldsymbol{\nabla} h \tag{21}$$

while the geostrophic transport relative to the bottom is given by

$$f\mathbf{k}\times(\mathbf{U}_g - h\mathbf{u}_g(-h)) \;=\; -\boldsymbol{\nabla}E - gh\rho(-h)\boldsymbol{\nabla}h \tag{22}$$

Hence, apart from the term arising from the (perturbation) bottom density, the potential energy is the pressure variable which is related to the geostrophic transport relative to the bottom (frequently called 'baroclinic transport').

As a consequence of the rigid lid approximation the bottom pressure is a diagnostic variable which is determined by a Poisson equation,

$$\boldsymbol{\nabla}\cdot h\boldsymbol{\nabla}P \;=\; h\nabla^2 P + \boldsymbol{\nabla}h\cdot\boldsymbol{\nabla}P \;=\; -\nabla^2 E + f\nabla^2\psi + \beta\frac{\partial\psi}{\partial y} + \boldsymbol{\nabla}\cdot(\boldsymbol{\tau}+\mathbf{F}) \tag{23}$$

This equation is used to compute P in BARBI .

In circumpolar applications the model domain has periodicity in one dimension. It is then convenient to analyze the budget of the barotropic momentum averaged around a closed contour $\mathcal{C}$, e.g. a latitude circle,

$$\oint_{\mathcal{C}} d\mathbf{s}\cdot\frac{\partial\mathbf{U}}{\partial t} \;=\; -\oint_{\mathcal{C}} d\mathbf{s}\cdot h\boldsymbol{\nabla}P + \oint_{\mathcal{C}} d\mathbf{s}\cdot(\boldsymbol{\tau}+\mathbf{F}) \tag{24}$$

where the line integral of the bottom pressure gradient and ocean depth appears. It is the *bottom formstress* which in partial balance with the friction terms controls the acceleration of the path mean momentum. Note that the E-pressure term does not contribute.

Notice that the bottom torque and the JEBAR term may be rephrased as $\mathcal{J}(P,h) = f\mathbf{u}_g(-h)\cdot\boldsymbol{\nabla}h$ or $\mathcal{J}(E,1/h) \;=\; (f/h^2)\;(\mathbf{U}_g - h\mathbf{u}_g(-h))\cdot\boldsymbol{\nabla}h$, respectively. Thus the torques relate to geostrophic transports across depth contours, a property shared by the planetary topographic Jacobian in (11) which in its topographic part is expressed as total transport across depth contours, $\mathcal{J}(\psi,f/h) = (\beta/h)\partial\psi/\partial x + (f/h^2)\mathbf{U}\cdot\boldsymbol{\nabla}h$. These relations make evident that both vorticity equations are connected by transport terms across depth contours: in fact adding the projection of the momentum balance (1) onto $(1/h^2)(\mathbf{k}\times\boldsymbol{\nabla}h)$ to the depth-averaged vorticity balance (11) yields $1/h$ times the depth-integrated balance (10). A further property becomes apparent as well: because the current is to a high degree geostrophic, $\mathbf{U}\approx\mathbf{U}_g$, and $h\mathbf{u}_g(-h)) \ll \mathbf{U}_g$ there will be approximate cancelation of the planetary-topographic Jacobian and JEBAR in (11).

We should mention that some of the relations in this section have previously been discussed in Olbers and Wübber (1991), Olbers *et al.* (1992), Mertz and Wright (1992) and Cane *et al.* (1998).

The vorticity equation (11), the balance (2) of potential energy and the baroclinic momentum balance (3) form a closed set of differential equations for the variables ψ, E and $\tilde{\mathbf{u}}$, determining the evolution of the flow. They are in fact used in the BARBI code (and either directly or implicitly implemented in most complete OGCMs with rigid lid approximation, see e.g. Bryan 1969). In addition to the usual kinematic and dynamic boundary conditions the equations must be supplemented by the integral constraint (to be taken around each island)

$$\oint_{island} d\mathbf{s}\cdot\boldsymbol{\nabla}P \;=\; \oint_{island} d\mathbf{s}\cdot\frac{1}{h}\left[-\mathbf{k}\times\boldsymbol{\nabla}\frac{\partial\psi}{\partial t} - \boldsymbol{\nabla}E + f\boldsymbol{\nabla}\psi + \boldsymbol{\tau}+\mathbf{F}\right] \;=\; 0 \tag{25}$$

to supply information about the value of the streamfunction on the boundaries of a multi-connected domain. The constraint guarantees the unique existence of the bottom pressure field which is then diagnosed using (23).

Appendix B. Diffusion, dissipation and bottom velocity

The balance (2) of potential energy is derived from a density equation

$$\frac{\partial \rho}{\partial t} + \left[\frac{1}{h}\mathbf{U} + \mathbf{u}'\right] \cdot \boldsymbol{\nabla}\rho + [W + w'] \left(\frac{\partial \rho}{\partial z} - \frac{N^2}{g}\right) = -\boldsymbol{\nabla} \cdot \mathbf{J}_\rho - \frac{\partial B_\rho}{\partial z} \tag{26}$$

by multiplication with z and vertical integration (see Olbers and Eden 2003). Note that ρ is the *perturbation* density, i.e. the *total* density is $\varrho = \bar{\varrho}(z) + \rho$. The above balance applies, however, to the total density: the three-dimensional flux vector $\mathbf{F}_\rho = (\mathbf{J}_\rho, B_\rho)$ is the *flux of total density*. This becomes important when parameterizations are considered. The horizontal flux $\mathbf{J}_\rho$ is mainly associated with eddies while the vertical component B_ρ contains contributions from eddies and small-scale turbulence (this latter part yields the buoyancy source (5)). We thus write $\mathbf{F}_\rho = (\mathbf{J}_\rho, B_\rho) = (\mathbf{J}_\rho, B_\rho)_{eddy} + (0, B_\rho)_{turb}$ and consider the GM form for the 3dim eddy flux (e.g. Griffies 2004),

$$(\mathbf{J}_\rho, B_\rho)_{eddy} = -K \left[\boldsymbol{\nabla}_z \varrho - \mathbf{n}_z s^2 \frac{\partial \varrho}{\partial z}\right] \tag{27}$$

with an eddy diffusivity K. Here $\mathbf{n}_z$ is the vertical unit vector and $\boldsymbol{\nabla}_z = (\boldsymbol{\nabla}, 0)$, and $\mathbf{s} = -\boldsymbol{\nabla}_z \varrho / \varrho_z = -\boldsymbol{\nabla}_z \rho / \varrho_z$ is the slope vector of the isopycnals. Note that that the eddy flux is aligned along the isopycnals. We require that no flux occurs by eddies through the bottom, thus $\mathbf{J}_\rho \cdot \boldsymbol{\nabla} h + B_\rho = 0$ at the bottom for the eddy part. Assuming, as usual for the GM eddy flux, that K vanishes at the top and the bottom, we find the source term

$$\mathcal{D}_{eddy} = \boldsymbol{\nabla} \cdot K \boldsymbol{\nabla} E + g \int_{-h}^{0} K s^2 \frac{\partial \varrho}{\partial z} dz \tag{28}$$

in the balance of potential energy E. We identify two terms: 1. divergence of a flux which is downgradient of E; and 2. a term arising form the tilts of the isopycnals which represents dissipation since $\partial \varrho / \partial z$ is negative for stable stratification. Note that the GM density flux results in dissipation and diffusion of potential energy.

In the BARBI balance (2) of potential energy we have implemented the downgradient flux, however, with a constant K. The dissipation term $\mathcal{D}$ only becomes zero if the isopycnals are flat which only occurs if $\rho = \rho(z)$. Implementing this term in BARBI is important but not straightforward. We chose a damping form, $\mathcal{D} = \mu E$, which causes a tendency towards $E = 0$ rather than $\rho = \rho(z)$. It dissipates the variance of E. The magnitude of μ is estimated as $10^{-9 \cdots -10}$ s^{-1} for the parameters of our experiments and an amplitude 10^4 m^{3}s^{-2} for the potential energy.

To aid the interpretation of the baroclinic velocity variable $\tilde{\mathbf{u}}$ we note that the combination $\mathbf{v} = \tilde{\mathbf{u}} + h^2 \mathbf{U}/3$ appearing in the potential energy balance (2) is simply $\mathbf{v} = \int_h^0 z^2 \mathbf{u} dz$, a velocity variable dominated by the deep range of depths. Furthermore, the divergence $\boldsymbol{\nabla} \cdot \mathbf{v}$ appearing in the potential energy balance relates to the integrated vertical velocity moment $\int_{-h}^0 z w dz$, also dominated by near bottom range of depth. From (1) and (3) we find the balance of $\mathbf{u}_b = 3\mathbf{v}/h^3$,

$$\frac{\partial \mathbf{u}_b}{\partial t} + f \mathbf{k} \times \mathbf{u}_b = -\boldsymbol{\nabla} P + \mathbf{F}/h + 3\tilde{\mathbf{F}}/h^3 \tag{29}$$

which shows the cancelation of the E-gradient term and the windstress between the barotropic and the baroclinic momentum balance. Evidently, as the geostrophic part of $\mathbf{u}_b$ is in balance with the bottom pressure gradient, we refer to this variable as bottom velocity.

References

Borowski, D. *The Antarctic Circumpolar Current: dynamics of a circumpolar channel with blocked geostrophic contours.* PhD thesis, University Bremen, 2003.

Borowski, D., Gerdes, R., and D. Olbers. Thermohaline and wind forcing of a circumpolar channel with blocked geostrophic contours. *J. Phys. Oceanogr.*, 32:2520–2540, 2002.

Bryan, K. A numerical method for the study of the world ocean. *J. Comput. Phys.*, 4:347–376, 1969.

Bryan, K. and M.D. Cox. The circulation of the World Ocean : a numerical study. Part I, A homogeneous model. *J. Phys. Oceanogr.*, 2:319–335, 1972.

Cai, W., and P.G. Baines. Interactions between thermohaline- and wind-driven circulations and their relevance to the dynamics of the Antarctic Circumpolar Current, in a coarse-resolution global ocean general circulation model. *J. Geophys. Res.*, 101:14073–14094, 1996.

Cane, M.A., Kamenkovich, V.M., and A. Krupitsky. On the utility and disutility of JEBAR. *J. Phys. Oceanogr.*, 28:519–526, 1998.

Cox, M.D. A baroclinic numerical model of the Word Ocean: Preliminary Results. In *Numerical Models of Ocean Circulation*, pages 107–120, Durham, New Hampshire, Oct. 17 – 20, 1972, 1975.

Gent, P.R., and J.C. McWilliams. Isopycnal mixing in ocean circulation models. *J. Phys. Oceanogr.*, 20:150–155, 1990.

Gent, P.R., W.G. Large, and F.O. Bryan. What sets the mean transport through Drake Passage? *J. Geophys. Res.*, 106:2693–2712, 2001.

Gill, A. E. A linear model of the Antarctic Circumpolar Current. *J. Fluid Mech.*, 32:465–488, 1968.

Gnanadesikan, A., and R. W. Hallberg. On the relationship of the Circumpolar Current to Southern Hemisphere winds in coarse resolution ocean models. *J. Phys. Oceanogr.*, 30:2013–2034, 2000.

Greatbatch, R.J., Fanning, A.F., Goulding, A.D., and S. Levitus. A diagnostic of interpentadal circulation changes in the North Atlantic. *J. Geophys. Res.*, 96:22009–22023, 1991.

Griffies, S. *Fundamentals of ocean climate models.* Princeton University Press, Princeton, 2004.

Han, Y.-J. A numerical World Ocean general circulation model. Part I. Basic design and barotropic experiment. *Dyn. Atmos. Oceans*, 8:107–140, 1984a.

Han, Y.-J. A numerical World Ocean general circulation model. Part II. A baroclinic experiment. *Dyn. Atmos. Oceans*, 8:141–172, 1984b.

Hidaka, K., and M. Tsuchiya. On the Antarctic Circumpolar Current. *J. Mar. Res.*, 12:214–222, 1953.

Holland, W.R. Baroclinic and topographic influences on the transport in western boundary currents. *Geophys. Fluid Dynamics*, 4:187–210, 1973.

Hughes, C.W., and de Cuevas, B.A. Why western boundary currents in realistic oceans are inviscid: A link between form stress and bottom pressure torques. *J. Phys. Oceanogr.*, 31:2871–2885, 2001.

Johnson, G.C., and H.L. Bryden. On the size of the Antarctic Circumpolar Current. *Deep-Sea Res.*, 36:39–53, 1989.

Johnson, J.A., and R.B. Hill. A three-dimensional model of the southern ocean with bottom topography. *Deep-Sea Res.*, 22:745–751, 1975.

Karsten, RH, Jones, H, Marshall, J. The role of eddy transfer in setting the stratification and transport of a Circumpolar Current. *J. Phys. Oceanogr.*, 32:39–54, 2002.

Klinck, J. M. Vorticity dynamics of seasonal variations of the Antarctic Circumpolar Current from a modeling study. *J. Phys. Oceanogr.*, 21:1515–1533, 1991.

Krupitsky, A., and M.A. Cane. On topographic pressure drag in a zonal channel. *J. Mar. Res.*, 52:1 – 23, 1994.

Krupitsky, A., and M.A. Cane. A two layer wind-driven ocen model in an multiply connected domain with bottom topography. *J. Phys. Oceanogr.*, 27:2395 – 2404, 1997.

Krupitsky, A., V.M. Kamekovich, N. Naik and M.A. Cane. A linear equivalent barotropic model of the Antarctic Circumpolar Current with realistic coastline and bottom topography. *J. Phys. Oceanogr.*, 26:1803–1824, 1996.

Levitus, S., and T. P. Boyer. *World Ocean Atlas 1994*. U.S. Department of Commerce, NOAA, NESDIS, 1994.

Marshall, J., Olbers, D., Ross, H., and D. Wolf-Gladrow. Potential vorticity constraints on the dynamics and hydrography in the Southern Ocean. *J. Phys. Oceanogr.*, 23:465–487, 1993.

Mellor, G.L., Mechoso, C.R., and N. Keto. A diagnostic calculation of the general circulation of the Atlantic Ocean. *Deep-Sea Res.*, 29:1171–1192, 1982.

Mertz, G., and D.G. Wright. Interpretations of the JEBAR term. *J. Phys. Oceanogr.*, 22:301–305, 1992.

Munk, W.H., and E. Palmén. Note on dynamics of the Antarctic Circumpolar Current. *Tellus*, 3:53–55, 1951.

Olbers, D. Comment on 'On the obscurantist physics of 'form drag' in theorizing about the Circumpolar Current. *J. Phys. Oceanogr.*, 28:1647–1654, 1998.

Olbers, D. On the role of eddy mixing on the transport of zonal ocean currents. In H. Baumert, J. Simpson, J. Sündermann, editor, *Marine Turbulence: Theories, Observations and Models*, pages 511–529, Berlin, 2005. Springer-Verlag.

Olbers, D, and C. Eden. A simplified general circulation model for a baroclinic ocean with topography. Part I: Theory, waves and wind-driven circulations. *J. Phys. Oceanogr.*, 33:2719–2737, 2003.

Olbers, D., and C. Völker. Steady states and variability in oceanic zonal flows. In D.L.T. Anderson and J. Willebrand, editor, *Decadal climate variability dynamics and predicition*, pages 407–443, Berlin, 1996. Springer-Verlag.

Olbers, D., and V.O. Ivchenko. On the meridional circulation and balance of momentum in the Southern Ocean of POP. *Ocean Dynamics*, 52:79–93, 2001.

Olbers, D., Borowski, D., Völker, C., and J.-O. Wolff. The dynamical balance, transport and circulation of the Antarctic Circumpolar Current. *Antarctic Science*, 16(4):439–470, 2004.

Olbers D., Wübber C., and Wolff J.O. The dynamical balance of wind and buoyancy driven circumpolar currents. Research report 32, Alfred-Wegener-Institut für Polar- und Meeresforschung, Bremerhaven, 1992.

Olbers, D.J., and C. Wübber. The role of wind and buoyancy forcing of the Antarctic Circumpolar Current. In M Latif, editor, *Strategies for Future Climate Research*, pages 161–191. Max-Planck-Institut fur Meteorologie, 1991.

Olbers, D.J., Wenzel, M., and J. Willebrand. The inference of North Atlantic circulation patterns from climatological hydrographic data. *Reviews of Geophysics*, 23(4):313–356, 1985.

Rhines, P. The dynamics of unsteady currents. In E. Goldberg, editor, *The Sea, Vol. VI*, pages 189–318, New York, 1977. Wiley.

Rhines, P.B. and W.R. Young. A theory of the wind-driven circulation. I. Mid-Ocean gyres. *J. Mar. Res.*, 40 (Suppl.):559–596, 1982.

Rintoul, S.R., C. Hughes and D. Olbers. The Antarctic Circumpolar Current system. In G. Siedler, J. Church and J. Gould, editor, *Ocean Circulation and Climate*, pages 271–302, New York, 2001. Academic Press.

Sarkisyan, A.S., and V.F. Ivanov. Joint effect of baroclinicity and bottom relief as an important factor in the dynamics of sea currents. *Akad. Nauk. Atmosph. Oceanic Phys.*, 7(2):173–188, 1971.

Völker, C. Momentum balance in zonal flows and resonance of baroclinic Rossby waves. *J. Phys. Oceanogr.*, 29:1666–1681, 1999.

Wang, L., and R.X. Huang. A linear homogeneous model of wind-driven circulation in a β-plane channel. *J. Phys. Oceanogr.*, 25:587 – 603, 1995.

Wolff, J.-O., Maier-Reimer, E. and Olbers, D.J. Wind-Driven flow over topography in a zonal β-plane channel: a quasi-geostrophic model of the Antarctic Circumpolar Current. *J. Phys. Oceanogr.*, 21(2):236–264, 1991.